Rare Met.
https://doi.org/10.1007/s12598-024-02621-z

RARE METALS

LETTER

Absence of ultrasonic-vibration-induced plasticity in metallic glacial glasses

Zhe Chen, Shuai Ren*, Jian Zhu, Jie Shen, Xin Li, He-Ting Zhang, Hong-Ji Lin, Sajad Sohrabi, Wen-Qing Ruan, Zhen-Xuan Zhang, Xiong Liang, Jiang Ma*, Jun Shen

Received: 31 July 2023 / Revised: 4 September 2023 / Accepted: 11 September 2023

Metallic glasses (MGs) have been found to exhibit unexpected ultrasonic-vibration-induced plasticity (UVIP), which provides a promising way to realize room temperature processing and molding of MGs. However, whether all MGs possessing UVIP remains a mystery. Here, we report that metallic glacial glasses (MGGs) which are a new glass state obtained through a liquid–liquid transition, show a different behavior without UVIP. While the as-cast $La_{65}Ni_{20}Al_{15}$ MG exhibits UVIP, consistent with conventional MGs, the MGG counterpart obtained by heat treatment exhibits brittleness under ultrasonic vibration loading. The MGG possesses higher α-relaxation and β-relaxation peak temperatures and a weaker boson heat capacity peak, indicating that it is more stable than the as-cast MG, consistent with its ultrastable nature. A schematic energy landscape is established accordingly. This work may provide new insights into the understanding of the ultrasonic plasticity of MGs as well as the nature of the MGGs.

Metallic glasses (MGs), also called as amorphous alloys, are a unique state with the disordering of atomic packing, which are generally formed by quenching molten liquid at a high cooling rate to avoid the crystallization process [1–4]. MGs possess excellent properties, including large elastic limit, high specific strength, good wear resistance and high corrosion resistance [5–10]. As a result, these alloys exhibit potential wide applications in various occasions ranging from medical devices to electronic equipment [11]. However, the size of bulk metallic glasses (BMGs) is generally limited to the centimeter scale [1–3]. Therefore, it is still a huge hurdle to overcome the size limitation of BMGs [12, 13]. Furthermore, MGs frequently exhibit brittleness due to the lack of crystal defects (e.g., dislocations) and localized plastic deformation in shear bands [14–17]. Recent studies have shown that rejuvenation is an important way to enhance the mechanical properties of MGs, in particular, the compression plasticity of MGs [6, 18, 19]. However, the brittleness of MGs still restricts their extensive applications.

Recently, an intriguing phenomenon has been reported in MGs that large compression plasticity takes place at room temperature (far below the glass transition temperature, T_g) under ultrasonic vibration (UV) loading, which means that a compression load together with an ultrasound at 20 kHz are applied on the sample simultaneously. [17, 20–22]. This ultrasonic-vibration-induced plasticity (UVIP) of MGs provides an opportunity to realize advanced processing such as room temperature welding or embossing in MGs, serving as a promising approach to overcome the size, compositional and especially forming limitations of BMGs in principle [20]. The origin of the

Supplementary Information The online version contains supplementary material available at https://doi.org/10.1007/s12598-024-02621-z.

Z. Chen, S. Ren*, J. Zhu, H.-T. Zhang, H.-J. Lin, S. Sohrabi, W.-Q. Ruan, Z.-X. Zhang, X. Liang, J. Ma*, J. Shen
Shenzhen Key Laboratory of High Performance Nontraditional Manufacturing, College of Mechatronics and Control Engineering, Shenzhen University, Shenzhen 518060, China
e-mail: shuai.ren@szu.edu.cn

J. Ma
e-mail: majiang@szu.edu.cn

J. Shen
Institute of Physics, Chinese Academy of Sciences, Beijing 100190, China

X. Li
School of Mechanical, Electrical and Information Engineering, Shandong University, Weihai 264209, China

Published online: 23 April 2024

UVIP is considered to be related to the inherent dynamic heterogeneity and UV-induced atomic-scale dilations in MGs, which lead to the final softening of the solid-like amorphous structure, resulting in an overall fluid-like behavior. Many MG systems have been found to exhibit the UVIP [17, 20–22]. However, since the properties of MGs are generally sensitive to many conditions including compositions, temperature and thermal history, it is still an open question whether the UVIP is a universal behavior of all kinds of MGs.

A polyamorphic phase transition between two distinct glass states has been reported in some MGs recently [23–30]. A new glassy phase in these MGs is called as metallic glacial glass (MGG), which is considered to be linked to a liquid–liquid phase transition in the molten liquid state and thus provide a new perspective to understand the microstructure and nature of MGs [27, 28]. The MGG possesses a higher glass transition temperature (T_g) and a less enthalpy change (i.e., smaller areas under exothermic peaks during heating) than that of the original one, so it is a thermodynamically more stable glass state [26, 27, 31]. It thus invites an interesting question: whether the MGGs as more stable glassy states can also exhibit UVIP or not?

In this work, we report that the MGGs exhibit a different behavior without showing UVIP. For two MGG compositions, $La_{65}Ni_{20}Al_{15}$ and $La_{32.5}Ce_{32.5}Co_{25}Al_{10}$, the as-cast MGs exhibit excellent UVIP. In contrast, the MGGs exhibit embrittlement under UV loading. A compositionally similar MG, $La_{60}Ni_{15}Al_{25}$ (which is a conventional MG with only one exothermic peak), exhibits UVIP with slight crystallization after heat treatment, ruling out the possibility of crystallization responsible for the ultrasonic brittleness of MGGs. MGGs are found to exhibit higher α-relaxation and β-relaxation peak temperatures and weaker boson peak capacity peak. These results reflect that MGGs are more stable than the as-cast state, which is consistent with the ultrastable glass nature of MGGs [26, 27]. This work may provide new insights into the nature of the MGGs as well as the mechanism underlying the ultrasonic plasticity of MGs.

Two MGG compositions, $La_{65}Ni_{20}Al_{15}$ (abbreviated as La65 hereafter) and $La_{32.5}Ce_{32.5}Co_{25}Al_{10}$ (abbreviated as LaCe hereafter), and one conventional MG composition $La_{60}Ni_{15}Al_{25}$ (abbreviated as La60 hereafter) were synthesized by arc melting. The amorphous structure was examined using X-ray diffraction of Cu-K_α radiation (XRD, Rigaku MiniFlex 600) and a scan rate of 2 rad·min^{-1} was used. The thermal behaviors were determined using differential scanning calorimetry (DSC, Perkin-Elmer DSC-8000) with a heating rate of 20 K·min^{-1}. The microscopic morphology and elemental distribution were characterized using a transmission electron microscope (TEM, FEI Titan Cubed Themis G2 300) with energy dispersive spectroscopy (EDS). The relaxation features were performed by the dynamic mechanical analyzer (DMA, TA DMA-Q850), the morphology of DMA samples was 20 mm × 1.5 mm × 2 mm. A single cantilever mode was employed. The specific heat C_p was measured in the Physical Property Measurement System (PPMS, Quantum Design dynaCool).

UV loading was performed by a self-developed ultrasonic setup with a frequency of 20 kHz. The strain amplitude of our ultrasonic equipment could be adjusted in a range of 4–40 μm, and an amplitude of 40 μm was used in this work. All specimens for UV loading were cylindrical samples with a diameter of 2 mm and a height of 2.5 mm. The high-speed camera has a frame rate of 4000 fps and was used to capture images of the UV process.

Figure 1 shows the glass features of the MGG composition of La65 at different heat treatment temperatures. The black curve in Fig. 1a is the DSC curve of the as-cast La65 sample, and the T_g is determined ~ 438 K. The as-cast sample shows a quite narrow supercooled liquid region of 10 K, and a sharp exothermic peak takes place with further heating above T_1 (i.e., the onset temperature of the first exothermic peak) ~ 448 K. Then, the as-cast samples were heated up to 463, 473 and 483 K at a heating rate of 10 K·min^{-1} and then cooled down at a cooling rate of 100 K·min^{-1} immediately. DSC results after heat treatment are shown in Fig. 1a. It is noted that the first exothermic peak gradually disappears and the supercooled liquid region expands with the heat treatment temperature increasing from 463 to 483 K. Meanwhile, XRD patterns after heat treatment in Fig. 1b all maintain halo peaks similar to those of the as-cast sample, which may suggest that these samples still possess a complete amorphous structure. More interestingly, the second halo peak enhances with the heat treatment temperature increasing, suggesting that phase change emerges in the heat-treated sample [28]. According to the references [27], it is a new glass phase, namely the MGG, that appears after heat treatment.

High-resolution electron micrograph and the corresponding diffraction pattern of the MGG sample heat-treated at 473 K are shown in Fig. 1c. The image indicates that the MGG still maintains an amorphous structure down to the atomic level. In addition, EDS patterns in Fig. 1d exhibit a homogenous element distribution, suggesting that the heat treatment does not cause obvious element segregation. As a result, the MGG state is determined in the heat-treated La65 samples.

As a new glass phase, it is of interest to explore its ultrasonic behavior. Figure 2a shows the schematic diagram of the UV loading equipment. The parameters of UV

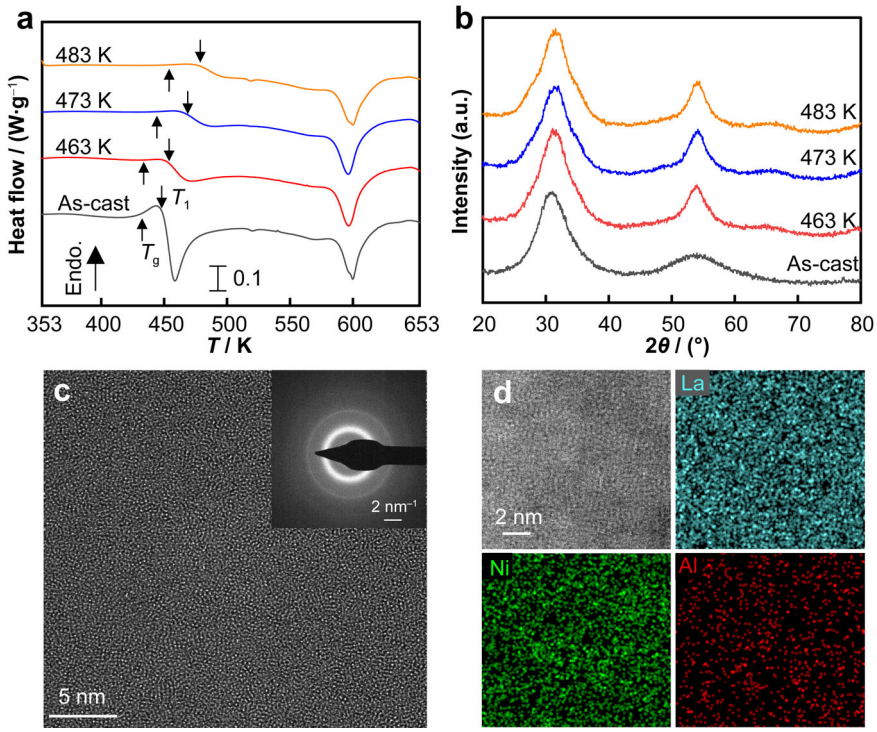

Fig. 1 Glass features of La65 alloys: **a** DSC curves of La65 alloys after heat treatment at temperatures ranging from 463 to 483 K, where up and down arrows illustrate T_g and T_1, respectively; **b** XRD patterns after heat treatment between 463 and 483 K; **c** HRTEM image of an MGG heat-treated at 473 K and (inset) corresponding SAED image; **d** EDS chemical mapping figures of MGG

loading can be referred to the experimental section. In each UV loading process, the ultrasonic sonotrode first descends at a constant speed to contact the sample. When the load exceeds the ultrasonic triggering threshold which is set as 16 MPa, the sonotrode starts to apply the ultrasonic vibrations to the sample, and the energy of each loading is 50 J. Figure 2b, c exhibits the sample pictures before and after the UV loading for the as-cast MG and MGG of La65 alloy respectively. The original sample in Fig. 2b is finally compressed into a thin disk, exhibiting a good UVIP, while the MGG sample in Fig. 2c breaks into pieces, displaying no UVIP. Figure 2d exhibits the sample pictures during UV loading taken by the high-speed camera (also refer to Supplementary Video S1). The top part of the as-cast sample becomes viscous-fluid-like at the very beginning of UV loading, and the sample continues deforming into a plate with the increase of time. In comparison, the MGG sample in Fig. 2e does not exhibit a fluid-like state but break into pieces under UV loading (also refer to Supplementary Video S2). The right figures in Fig. 2b, c show the load change with time in the process of UV loading for the as-cast MG and MGG respectively. The as-cast sample exhibits a low load around 50 MPa and never reaches to zero. In comparison, the load of the MGG sample decreases to zero suddenly in the middle, which corresponds to the occasion when the MGG sample fractures.

According to Figs. 1, 2, it is clear that the MGG in La65, as a new amorphous phase, does not display plasticity under UV loading, distinct from the UVIP behavior of the as-cast MG. However, it is still unclear whether the absence of UVIP is a universal behavior of MGGs. To check whether it is a common behavior, we performed the same experiment on another MGG composition $La_{32.5}Ce_{32.5}Co_{25}Al_{10}$ (LaCe). As shown in Fig. S1, the as-cast MG of LaCe exhibits UVIP, whereas there is no UVIP in MGG. As a result, it seems that the absence of ultrasonic plasticity is a common behavior of MGGs.

Since the MGGs are obtained by heat-treating the sample above T_g, there may be some doubts on the existence of nanocrystals in the heat-treated sample, and thus the influence of crystallization on the ultrasonic behavior must be taken into consideration. Thus, the ultrasonic behavior of a conventional amorphous alloy (La60) with a similar composition to La65 but without an MGG phase was studied.

Figure 3a exhibits DSC curve of the as-cast MG sample of La60, in which only one single exothermic peak takes place. The XRD pattern of the as-cast sample shows an amorphous structure. After the heat treatment at 483 K for 30 min, a sharp peak appears in the XRD pattern, indicating that slight crystallization occurs in the heat-treated sample. Figure 3b shows the sample picture before and

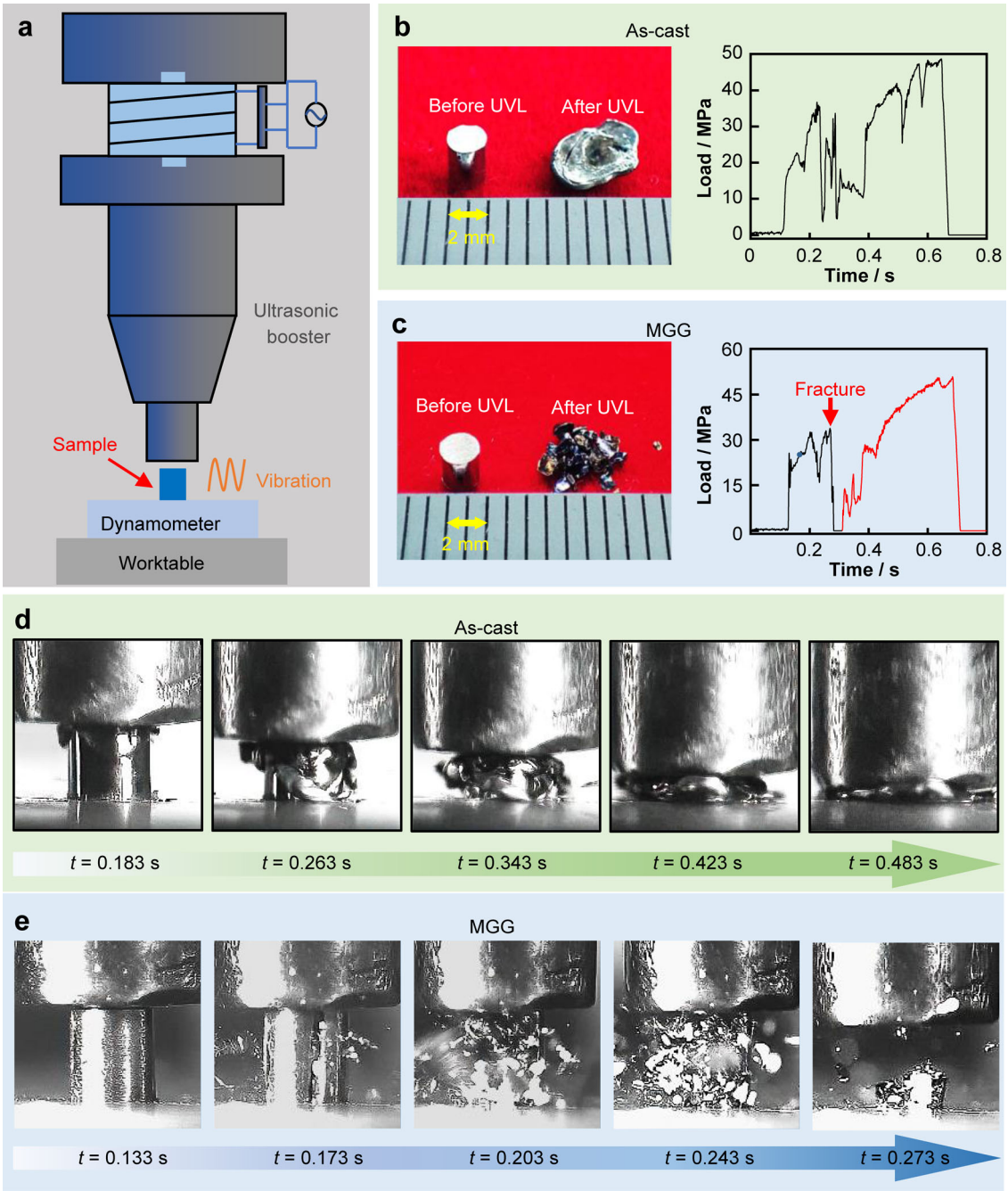

Fig. 2 Comparison of ultrasonic behavior of as-cast MG and MGG sample (heat-treated at 473 K) of La65: **a** schematic diagram of ultrasonic equipment; **b** sample picture before and after UV loading of as-cast MG sample and corresponding load curve as a function of time; **c** sample picture before and after UV loading of MMG sample and corresponding load change, where red arrow illustrates time point when sample cracks; sample pictures of high-speed camera of **d** as-cast MG and **e** MGG during UV loading

after the UV loading for the heat-treated La60 sample, and UVIP can be clearly observed. Figure 3c shows the load change with time. The load is at the same level as that of the as-cast La65 sample in Fig. 2b. The sample picture during the UV loading is shown in Fig. 3d (also refer to Video S3). A fluid-like deformation is observed, similar to the behavior of the as-cast La65 sample in Fig. 2b.

The results in Fig. 3 indicate that a slight crystallization does not destroy the ultrasonic plastic deformation ability of the conventional MGs. However, no obvious crystalline phase is observed in MGG samples according to XRD and TEM results in Fig. 1 and the results in the references [27, 28]. Hence, even if there were some nanocrystals in MGGs, they could not largely damage the ultrasonic

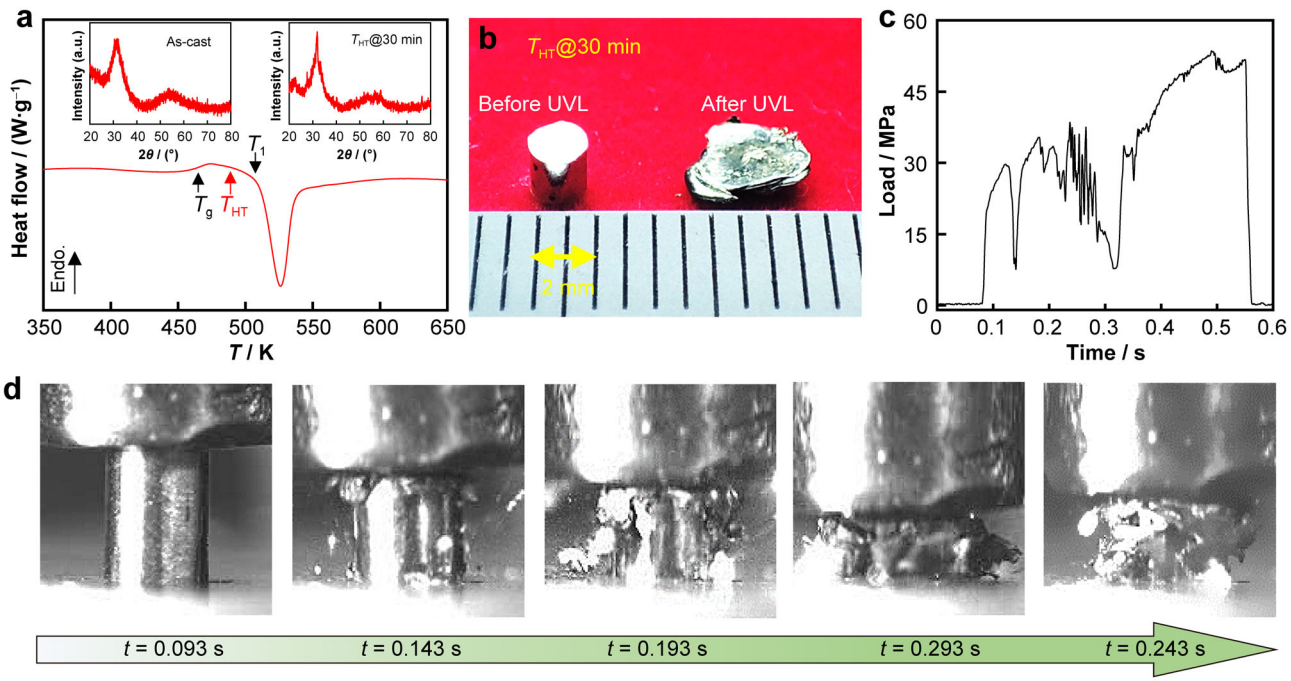

Fig. 3 Ultrasonic behavior of La60 with crystallization: **a** DSC curve of an as-cast sample together with XRD patterns before and after heat treatment, where treatment temperature (labeled as T_{HT}) is 483 K ($T_{HT} = T_g + 30$ K), aged time is 30 min; **b** photographs of aged sample before and after UV loading; **c** load as a function of time for aged sample during UV loading; **d** high-speed camera photographs of aged sample during UV loading

plasticity. As a result, the influence of crystallization on the ultrasonic brittleness of MGGs can be excluded.

The exclusion of the influence of crystallization suggests that the absence of UVIP is an intrinsic feature of MGGs. Thus, it is worth exploring the underlying mechanism behind the ultrasonic brittleness of MGGs, which may provide new clues to understand the nature of MGGs. Figure 4a shows the loss modulus curves of the as-cast MG and MGG of La65, in which frequencies of 0.2, 0.4, 1, 2, 4, 10 and 20 Hz are used. Two relaxation peaks can be observed in their curves: the low temperature peak is the β-relaxation peak and the high temperature one corresponds to the α-relaxation. The peak temperatures of both α-relaxation and β-relaxation of the MGG are higher than those of the as-cast one. The peak temperature increase of the β-relaxation is ~ 24 K, while the increase of the α-relaxation is up to 40 K. The peak temperature increase indicates that the MGG is more stable than the as-cast one in energy.

Figure 4b shows the relation of frequency (f) and peak temperature (T_β) of β-peaks in both as-cast MG and MGG, which are well fitted by an Arrhenius relation:

$$f = f_0 \cdot \exp(-E_a/RT_\beta) \quad (1)$$

where f_0 is the prefactor, E_a is an apparent activation energy of β-relaxation and R is the gas constant. The E_a of the as-cast MG and MGG are yielded (75.4 ± 2.3) and (88.7 ± 1.8) kJ·mol^{-1}, respectively. A higher E_a of the MGG means that it is harder to activate the β-relaxation in the MGG.

It is well known that the MGs all exhibit a unique boson vibrational anomaly, i.e., an excess of low-frequency vibrations over Debye contributions at the level of 1 THz, different from the crystalline counterpart [32–34]. This anomaly is referred to as the boson peak, which is a peak upon plotting the reduced density of states $g(\omega)/\omega^2$ over ω (ω is the frequency) ~ 1 THz, and can also be manifested by a peak in the specific heat (C_p) at 5–20 K in a plot of C_p/T^3 vs. T. Similar anomaly has also been found in other disordered solids [35–37]. The boson peak of MGs is generally believed to stem from the localized loosely packed regions in MGs [38]. Thus, the peak intensity and peak temperature can also reflect the relative stability of the as-cast MG and MGG.

We thus performed specific heat measurements of the as-cast and MGG samples of La65 and LaCe alloys (the data for LaCe samples are shown in Fig. S2). For non-magnetic alloys, the low temperature specific heat mainly comes from the contribution of electrons and phonons. In order to obtain the contribution of phonons, we need to remove the contribution of electrons. According to the textbook [39], the electron specific heat is proportional to temperature, while the phonon specific heat is proportional to the cube of temperature. Thus, the low temperature C_p data can be fitted by:

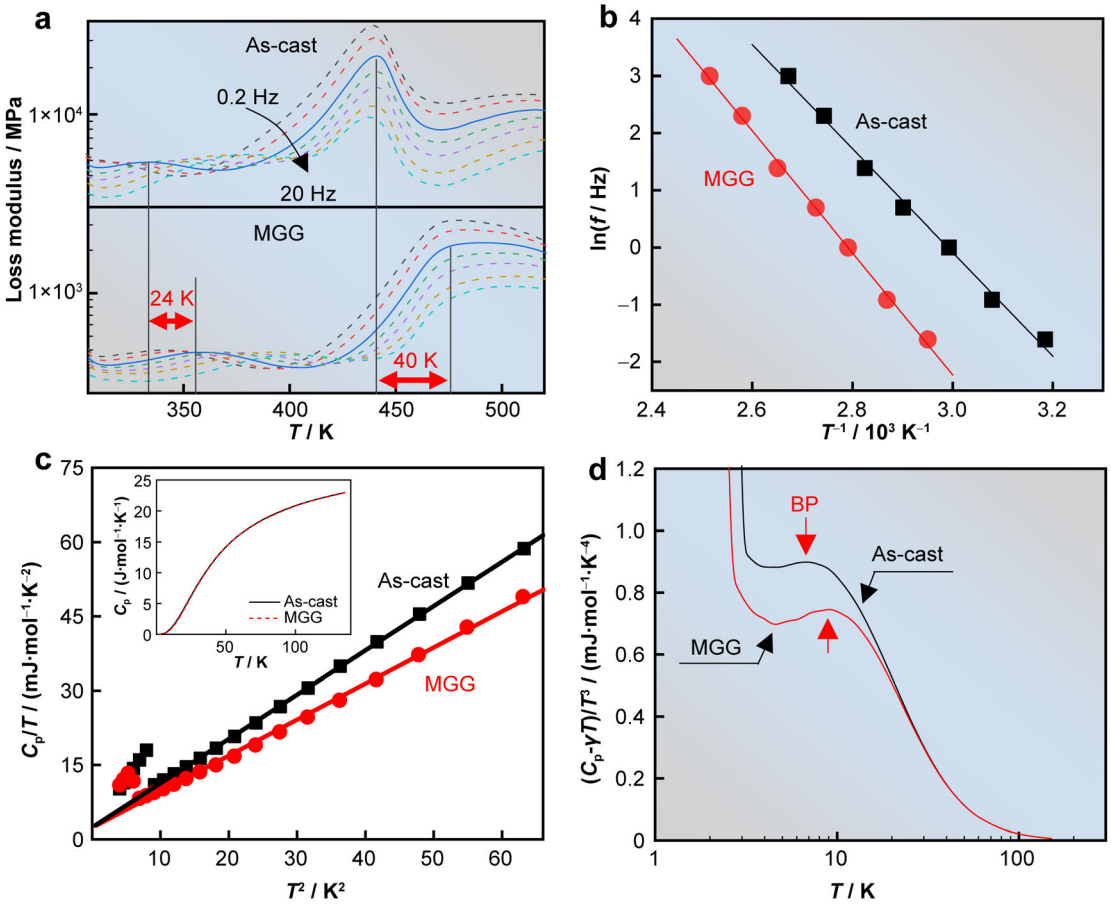

Fig. 4 Dynamic features of as-cast MG and MGG of La65. **a** Loss modulus curves of MG and MGG (heat-treated at 463 K) at frequencies of 0.2, 0.4, 1, 2, 4, 10 and 20 Hz; **b** Arrhenius plots of peak temperature and frequency of β-relaxation; **c** plots of C_p/T vs. T^2 from 2 to 8 K, where solid lines are obtained by fitting and (inset) curves of C_p vs. T of La65; **d** curves of $(C_p\text{-}\gamma T)/T^3$ vs. T for La65, where BP is labeled by red arrows

$$C_p/T = \gamma + \beta T^2 \quad (2)$$

where γ is the calorimetric linear coefficient corresponding to electronic contributions, and β is the calorimetric cubic coefficient [39]. Figure 4c exhibits a scatter plot of C_p/T vs. T^2 between 2 and 8 K of both as-cast MG and MGG in La65 alloys. The corresponding specific heat curves from 150 to 2 K are shown in the inset of Fig. 4c. In Fig. 4c, it is found that the data can be well fitted by Eq. (2), except for sharp peaks below 10 K^2, which are caused by superconducting transitions [38]. As a consequence, the contribution of electrons can be eliminated.

Then, the $(C_p\text{–}\gamma T)/T^3$ as a function of T for La65 is shown in Fig. 4d. Humps can be clearly seen around 10 K in the two curves, which are the boson peaks. It is noted that the boson peak of the MGG exhibits a lower magnitude and shifts to a higher temperature than that of the as-cast one. The weaker boson peak also indicates that the MGG is more stable than the as-cast MG.

According to the data in Fig. 4, it is clear that the MGG is a more stable state than the as-cast one. These results are consistent with the fact that the MGG actually is a thermodynamically ultrastable glass state, owing to its higher T_g and much lower enthalpy change [27]. Accordingly, we tried to explain the absence of UVIP of MGGs from the view of potential energy landscape (PEL). Figure 5 exhibits the schematic PEL diagram, in which several potential energy minima/megabasins between different configurations are illustrated. The deepest energy minima on the PEL corresponds to the stable crystalline phases. During the rapid cooling of the melt, these deep and narrow minima cannot be reached due to energy barriers, resulting in the formation of as-cast MGs [4, 26, 40]. The as-cast MGs are generally high energy states, since the system is readily trapped in many relatively high-energy metastable megabasins [4, 40]. However, the MGG formation process is accompanied by energy release, and thus the MGG is relatively stable, locating in another lower potential energy basin on the PEL. Higher energy is demanded to excite the system to other states with higher potential energy. As a result, the UV loading fractures the MGG before it can be excited to higher energy state during

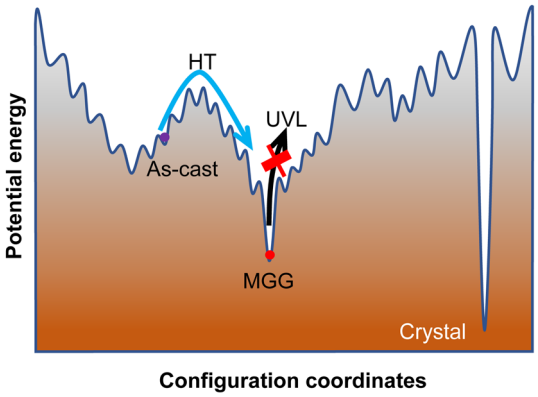

Fig. 5 Schematic diagram of PEL containing MGG

the loading process. That is, the MGG cracks before it softens and thus does not exhibit UVIP.

In recent years, experts have made significant diskoveries regarding liquid–liquid phase transitions in various systems, including Fe-based [41] and Mg-based [42] MGs. These findings have provided us with a better understanding of the nature of glass. Additionally, we have observed that MGG does not exhibit UVIP under UV-loading, which offers a unique perspective for comprehending the liquid–liquid phase transition in MG.

It is important to note that the explanation regarding to the energy landscape in this work is merely a qualitative explanation. This theory has limitations in terms of its phenomenological nature and inability to quantitatively describe many issues related to amorphous and glass transitions. Moreover, obtaining an accurate energy barrier for a particular system is challenging, making it difficult to connect energy barriers with specific real-world systems. Therefore, additional efforts are required to establish a theoretical model that can explain the different ultrasonic-vibration-inducec behaviors observed in MGGs as compared to conventional MGs. Fortunately, some reliable multiscale computational methods have been proposed, which can potentially contribute to future theoretical studies on this topic [43–45].

In summary, we have found that the MGGs exhibit a unique behavior without UVIP, distinct from the conventional MGs. Crystallization is excluded to be responsible for the ultrasonic brittleness of the MGGs, indicating that the absence of UVIP is an intrinsic property of MGGs. MGGs possess higher α-relaxation and β-relaxation peak temperatures and a weaker boson heat capacity peak, so they are more stable than the corresponding as-cast MGs, consistent with the ultrastable nature of the MGGs. According to their ultrastable nature, a schematic energy landscape is established to explain the absence of UVIP of the MGGs. This work not only sheds new light on the understanding of the ultrasonic plasticity of MGs, but also provides a new perspective to explore the nature of MGGs.

Acknowledgements This study was financially supported by the Key Basic and Applied Research Program of Guangdong Province, China (No. 2019B030302010), the National Natural Science Foundation of China (Nos. 52371160, 51901243, 52122105 and 51971150), the National Key Research and Development Program of China (No. 2018YFA0703604). The authors also thank the assistance on microscope observation received from the Electron Microscope Center of the Shenzhen University.

Declarations

Conflict of interests The authors declare that they have no conflict of interests.

References

[1] Berthier L, Biroli G. Theoretical perspective on the glass transition and amorphous materials. Rev Mod Phys. 2011;83(2):587. https://doi.org/10.1103/RevModPhys.83.587.
[2] Ediger MD, Angell CA, Nagel SR. Supercooled liquids and glasses. J Phys Chem-Us. 1996;100(31):13200. https://doi.org/10.1021/jp953538d.
[3] Chen MW. A brief overview of bulk metallic glasses. NPG Asia Mater. 2011;3(9):82. https://doi.org/10.1038/asiamat.2011.30.
[4] Debenedetti PG, Stillinger FH. Supercooled liquids and the glass transition. Nature. 2001;410(6825):259. https://doi.org/10.1038/35065704.
[5] Tian L, Cheng YQ, Shan ZW, Li J, Wang CC, Han XD, Sun J, Ma E. Approaching the ideal elastic limit of metallic glasses. Nat Commun. 2012;3:609. https://doi.org/10.1038/ncomms1619.
[6] Pan J, Ivanov YP, Zhou WH, Li Y, Greer AL. Strain-hardening and suppression of shear-banding in rejuvenated bulk metallic glass. Nature. 2020;578(7796):559. https://doi.org/10.1038/s41586-020-2016-3.
[7] Hofmann DC, Suh JY, Wiest A, Duan G, Lind ML, Demetriou MD, Johnson WL. Designing metallic glass matrix composites with high toughness and tensile ductility. Nature. 2008;451(7182):1085. https://doi.org/10.1038/nature06598.
[8] Jang D, Greer JR. Transition from a strong-yet-brittle to a stronger-and-ductile state by size reduction of metallic glasses. Nat Mater. 2010;9(3):215. https://doi.org/10.1038/nmat2622.
[9] Li MX, Zhao SF, Lu Z, Hirata A, Wen P, Bai HY, Chen M, Schroers J, Liu Y, Wang WH. High-temperature bulk metallic glasses developed by combinatorial methods. Nature. 2019;569(7754):99. https://doi.org/10.1038/s41586-019-1145-z.
[10] Wang WH. Bulk metallic glasses with functional physical properties. Adv Mater. 2009;21(45):4524. https://doi.org/10.1002/adma.200901053.
[11] Wang WH, Dong C, Shek CH. Bulk metallic glasses. Mat Sci End R. 2004;44(2):45. https://doi.org/10.1016/j.mser.2004.03.001.
[12] Li HZ, Li Z, Yang J, Ke HB, Sun BA, Yuan CC, Ma J, Shen J, Wang WH. Interface design enabled manufacture of giant metallic glasses. Sci China Mater. 2021;64(4):964. https://doi.org/10.1007/s40843-020-1561-x.
[13] Li R, Pang SJ, Ma CL, Zhang T. Influence of similar atom substitution on glass formation in (La-Ce)-Al-Co bulk metallic glasses. Acta Mater. 2007;55(11):3719. https://doi.org/10.1016/j.actamat.2007.02.026.

[14] Das A, Kagebein P, Küchemann S, Maaß R. Temperature rise from fracture in a Zr-based metallic glass. Appl Phys Lett. 2018; 112: 261905. https://doi.org/10.1063/1.5034762.
[15] Zhou D, Li BJ, Zhang SY, Hou B, Li YL. Rate-dependent shear banding and fracture behavior in a ductile bulk metallic glass. Mat Sci Eng A-Struct. 2018;730:270. https://doi.org/10.1016/j.msea.2018.05.066.
[16] Li PY. Effects of strain rates on shear band and serrated flow in a bulk metallic glass. J Non-Cryst Solids. 2018;484:30. https://doi.org/10.1016/j.jnoncrysol.2018.01.012.
[17] Sun F, Wang B, Luo F, Yan YQ, Ke HB, Ma J, Shen J, Wang WH. Shear punching of bulk metallic glasses under low stress. Mater Design. 2020;190:108595. https://doi.org/10.1016/j.matdes.2020.108595.
[18] Ketov SV, Sun YH, Nachum S, Lu Z, Checchi A, Beraldin AR, Bai HY, Wang WH, Louzguine-Luzgin DV, Carpenter MA, Greer AL. Rejuvenation of metallic glasses by non-affine thermal strain. Nature. 2015;524(7564):200. https://doi.org/10.1038/nature14674.
[19] Sun YH, Concustell A, Greer AL. Thermomechanical processing of metallic glasses: extending the range of the glassy state. Nat Rev Mater. 2016;1(9):1. https://doi.org/10.1038/natrevmats.2016.39.
[20] Ma J, Yang C, Liu XD, Shang BS, He QF, Li FC, Wang TY, Wei D, Liang X, Wu X, Wang YJ, Gong F, Guan PF, Wang WH, Yang Y. Fast surface dynamics enabled cold joining of metallic glasses. Sci Adv. 2019;5(11):eaax7256. https://doi.org/10.1126/sciadv.aax7256.
[21] Li X, Wei D, Zhang JY, Liu XD, Li Z, Wang TY, He QF, Wang YJ, Ma J, Wang WH, Yang Y. Ultrasonic plasticity of metallic glass near room temperature. Appl Mater Today. 2020;21: 100866. https://doi.org/10.1016/j.apmt.2020.100866.
[22] Zhao H, Sun F, Li X, Ding Y, Yan YQ, Tong X, Ma J, Ke HB, Wang WH. Ultrastability of metallic supercooled liquid induced by vibration. Scripta Mater. 2021;194:113606. https://doi.org/10.1016/j.scriptamat.2020.10.048.
[23] Sheng HW, Liu HZ, Cheng YQ, Wen J, Lee PL, Luo WK, Shastri SD, Ma E. Polyamorphism in a metallic glass. Nat Mater. 2007;6(3):192. https://doi.org/10.1038/nmat1839.
[24] Li G, Wang YY, Liaw PK, Li YC, Liu RP. Electronic structure inheritance and pressure-induced polyamorphism in lanthanide-based metallic glasses. Phys Rev Lett. 2012;109(12): 125501. https://doi.org/10.1103/PhysRevLett.109.125501.
[25] Du Q, Liu XJ, Fan HY, Zeng QS, Wu Y, Wang H, Chatterjee D, Ren Y, Ke Y, Voyles PM, Lu ZP, Ma E. Reentrant glass transition leading to ultrastable metallic glass. Mater Today. 2020; 34:66. https://doi.org/10.1016/j.mattod.2019.09.002.
[26] Lou HB, Zeng ZD, Zhang F, Chen SY, Luo P, Chen XH, Ren Y, Prakapenka VB, Prescher C, Zuo XB, Li T, Wen JG, Wang WH, Sheng HW, Zeng QS. Two-way tuning of structural order in metallic glasses. Nat Commun. 2020;11(1):314. https://doi.org/10.1038/s41467-019-14129-7.
[27] Shen J, Lu Z, Wang JQ, Lan S, Zhang F, Hirata A, Chen MW, Wang XL, Wen P, Sun YH, Bai HY, Wang WH. Metallic glacial glass formation by a first-order liquid-liquid transition. J Phys Chem Lett. 2020;11(16):6718. https://doi.org/10.1021/acs.jpclett.0c01789.
[28] Luan H, Zhang X, Ding H, Zhang F, Luan JH, Jiao ZB, Yang YC, Bu H, Wang R, Gu J, Shao C, Yu Q, Shao Y, Zeng Q, Chen N, Liu CT, Yao KF. High-entropy induced a glass-to-glass transition in a metallic glass. Nat Commun. 2022;13(1):2183. https://doi.org/10.1038/s41467-022-29789-1.
[29] Lan S, Ren Y, Wei XY, Wang B, Gilbert EP, Shibayama T, Watanabe S, Ohnuma M, Wang XL. Hidden amorphous phase and reentrant supercooled liquid in Pd-Ni-P metallic glasses. Nat Commun. 2017;8:14679. https://doi.org/10.1038/ncomms14679.
[30] Shen J, Liu SL, Sun Y, Wang WH. Metallic glacial glass. Natl Sci Open. 2023;2(3):20220049. https://doi.org/10.1360/nso/20220049.
[31] Yu HB, Luo Y, Samwer K. Ultrastable metallic glass. Adv Mater. 2013;25(41):5904. https://doi.org/10.1002/adma.201302700.
[32] Phillips WA, editor. Amorphous Solids: Low Temperature Properties. Berlin Heidelberg: Springer-Verlag; 1981. 1.
[33] Wang WH. Dynamic relaxations and relaxation-property relationships in metallic glasses. Prog Mater Sci. 2019;106: 100561. https://doi.org/10.1016/j.pmatsci.2019.03.006.
[34] Lunkenheimer P, Schneider U, Brand R, Loid A. Glassy dynamics. Contemp Phys. 2010;41(1):15. https://doi.org/10.1080/001075100181259.
[35] Remenyi G, Sahling S, Biljakovic K, Staresinic D, Lasjaunias JC, Lorenzo JE, Monceau P, Cano A. Incommensurate systems as model compounds for disorder revealing low-temperature glasslike behavior. Phys Rev Lett. 2015;114(19):195502. https://doi.org/10.1103/PhysRevLett.114.195502.
[36] Gebbia JF, Ramos MA, Szewczyk D, Jezowski A, Krivchikov AI, Horbatenko YV, Guidi T, Bermejo FJ, Tamarit JL. Glassy anomalies in the low-temperature thermal properties of a minimally disordered crystalline solid. Phys Rev Lett. 2017;119(21): 215506. https://doi.org/10.1103/PhysRevLett.119.215506.
[37] Ren S, Zong HX, Tao XF, Sun YH, Sun BA, Xue DZ, Ding XD, Wang WH. Boson-peak-like anomaly caused by transverse phonon softening in strain glass. Nat Commun. 2021;12(1): 5755. https://doi.org/10.1038/s41467-021-26029-w.
[38] Huang B, Zhu ZG, Ge TP, Bai HY, Sun BA, Yang Y, Liu CT, Wang WH. Hand in hand evolution of boson heat capacity anomaly and slow β-relaxation in La-based metallic glasses. Acta Mater. 2016;110:73. https://doi.org/10.1016/j.actamat.2016.03.016.
[39] Srivastava GP. Physics of phonons. New York: Taylor & Francis Group; 1990.1.
[40] Zhao Y, Shang B, Zhang B, Tong X, Ke H, Bai H, Wang WH. Ultrastable metallic glass by room temperature aging. Sci Adv. 2022;8(33):eabn3623. https://doi.org/10.1126/sciadv.abn3623.
[41] Ge JC, He HY, Zhou J, Lu CY, Dong WX, Liu SN, Lan S, Wu ZD, Wang AD, Wang L, Yu C, Shen BL, Wang XL. In-situ scattering study of a liquid-liquid phase transition in Fe-B-Nb-Y supercooled liquids and its correlation with glass-forming ability. J Alloys Compd. 2019;787:831. https://doi.org/10.1016/j.jallcom.2019.02.114.
[42] Li KH, Ge JC, Liu SN, Fu S, Yin ZX, Zhang WT, Chen GX, Wei SC, Ji H, Feng T, Liu Q, Wang XL, Zuo XB, Ren Y, Hahn H, Lan S. In situ scattering study of multiscale structural evolution during liquid-liquid phase transition in Mg-based metallic glasses. Rare Met. 2021;40(11):3107. https://doi.org/10.1007/s12598-021-01767-4.
[43] Han KM, Jiang H, Wang YM, Qiang JB. Zr-Ti-Al-Fe-Cu bulk metallic glasses for biomedical device application. Rare Met. 2021;40(5):1239. https://doi.org/10.1007/s12598-020-01644-6.
[44] Talebi H, Silani M, Bordas SPA, Kerfriden P, Rabczuk T. A computational library for multiscale modeling of material failure. Comput Mech. 2013;53(5):1047. https://doi.org/10.1007/s00466-013-0948-2.
[45] Vu-Bac N, Lahmer T, Zhuang X, Nguyen-Thoi T, Rabczuk T. A software framework for probabilistic sensitivity analysis for computationally expensive models. Adv Eng Softw. 2016;100: 19. https://doi.org/10.1016/j.advengsoft.2016.06.005.